Supporting Information

500 nm induced tunable syngas synthesis from CO_2 photoreduction by controlling heterojunction concentration

Conghui Qiu,[a] Xiaojie Hao,[a] Ling Tan,[a] Xian Wang,[a] Wenjing Cao,[a] Junyan Liu,[a] Yufei Zhao,[a]* Yu-Fei Song[a]*

[a]*State Key Laboratory of Chemical Resource Engineering and Beijing Advanced Innovation Center for Soft Matter Science and Engineering, Beijing University of Chemical Technology, Beijing, 100029, People's Republic of China.*

Experiment Section

Materials: $Co(NO_3)_2 \cdot 6H_2O$, $Al(NO_3)_3 \cdot 9H_2O$, NaOH, urea and ammonium heptamolybdate were purchased from Energy Chemical and used without further purification. All water used in the experiment was deionized and decarbonated to avoid the influence of gas dissolved in liquid.

The synthesis of ultrathin CoAl-LDH nanosheet (denoted as U-CoAl-LDH): The formation process of ultrathin CoAl-LDH nanosheet was illustrated in Scheme S1 (Step 1), typically, by double drop co-precipitation[1] of salt (n $(Co(NO_3)_2 \cdot 6H_2O)$/n $(Al(NO_3)_3 \cdot 9H_2O)$ = 2:1) (50 mM nitrate solution) and alkali solution (0.25 M NaOH) to 20 mL aqueous solution holding pH around 10 under magnetic stirring at 80 ℃. After centrifuging and washing with water, the sample can be obtained with a light pink color.

The synthesis of ultrathin MoS_2 nanosheet (denoted as U-MoS_2): The formation process of oxygen-incorporated ultrathin MoS_2 was schematically illustrated in Scheme S1 (Step 2). Briefly, MoS_2 was synthesized by the hydrothermal method[2] under 180 ℃ for 24 h with ammonium heptamolybdate and thiourea as precursors dissolved in 45 mL deionized water. After centrifuging and washing with water and ethanol, the dark grey sample was collected.

The synthesis of CoAl-LDH/MoS_2 nanocomposite (denoted as LDH/MoS_2): The formation process of CoAl-LDH/MoS_2 nanocomposite was schematically illustrated in Scheme S1 (Step 3). U-CoAl-LDH and U-MoS_2 with the mass fraction of 92.5% and 7.5%, respectively, were dissolved in aqueous solution by gradually dropping the MoS_2 nanosheet suspension into the CoAl-LDH suspension, and magnetically stirred over 48 h. Positively charged U-CoAl-LDH nanosheet and negatively charged U-MoS_2 nanosheet were electrostatically self-assembled in aqueous solution to obtain LDH/MoS_2 nanocomposite. The color of the solution changed gradually from light pink to purplish gray and then dark gray gradually. Finally, through low-speed centrifugation, the supernatant was transparent, indicating the nanocomposite was successfully synthesized.

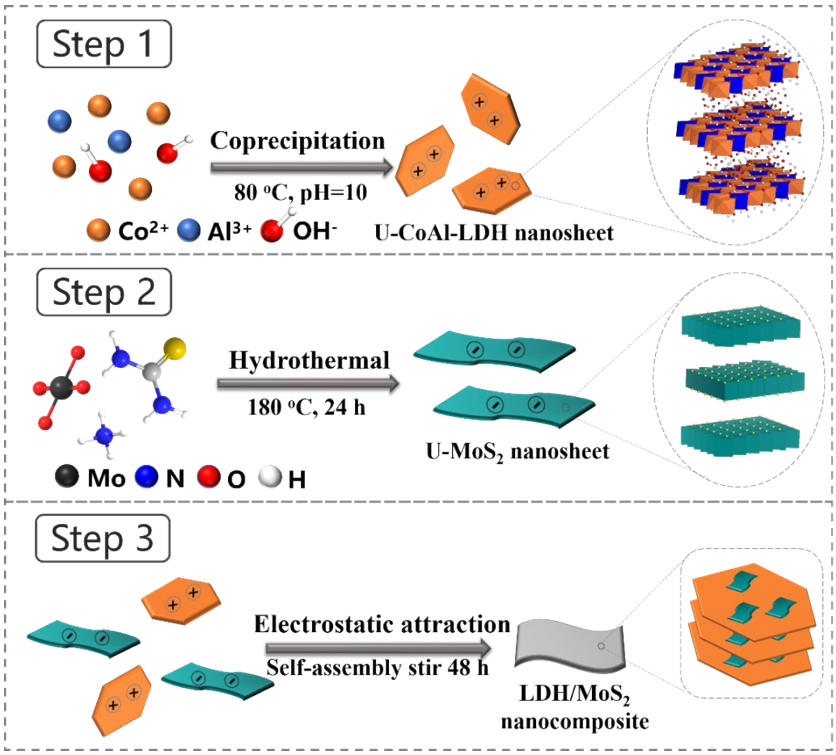

Scheme S1. Schematic illustration for the synthesis of U-CoAl-LDH, U-MoS_2 and

LDH/MoS_2 nanocomposite, respectively.

Materials Characterization

The powder X-ray diffraction (XRD) pattern was conducted on a Bruker D8-Advance X-ray diffractometer over the 2θ range of 3-70° with Cu Kα as radiation (λ = 1.5405 Å). The UV−vis DRS was collected over the range of 200-800 nm using a Beijing PGENERAL TU-1901 spectrometer with $BaSO_4$ as reference. High-resolution Transmission electron microscopy (HRTEM) and scanning electron microscopy (SEM) images appeared on a JEOL JEM-2010 electron microscope operating at 200 kV and a Zeiss Supra 55. The Mo and Co K-edge X-ray absorption near edge structure (XANES) and extended X-ray absorption fine structure (EXAFS) measurements were obtained at the 1W1B beamline stem from Beijing synchrotron radiation facility under room temperature. Fourier transform EXAFS (FT-EXAFS) shell fitting was carried out with Artemis Software.[3] X-ray photoelectron spectroscopy (XPS) measurements were tested out with monochromatized Al Kα exciting X-ray radiation (PHI Quantera SXM) and calibrated against C 1s at 284.8 eV. The Fourier transform infrared (FT-IR) spectra of the catalysts were carried out on the Perkin Elmer FTIR spectrum in the range of 400-4000 cm^{-1} using a KBr pellet. Raman spectroscopy was obtained at a Jobin-Yvon LabRam HR800 microscope. Photoluminescence (PL) spectra of the samples were tested at room temperature on a steady-state spectrofluorometer (SHIMADZU RF-6000) with an excitation wavelength of 400 nm and an emission wavelength of 632 nm.

Photocatalytic CO_2 reduction test

In order to test the performance of photocatalytic CO_2 reduction reaction, we used a 40 mL closed stainless steel photoreactor with a Quartz cover for light irradiation. The reactions were tested under mild conditions with 0.2-1.5 mg/mL photocatalysts, 10 mL mixed solution with H_2O:CH_3CN:TEOA=1:3:1 (v/v/v), and 3.3 mg $[Ru(bpy)_3]Cl_2 \cdot 6H_2O$. Before irradiation, the reaction equipment was vacuum-treated and purged with high purity CO_2 (Beijing Beiwen Gas Comp. 99.999 %) gas until the pressure reached 1.8 bar in the photoreactor. Then repeated the above steps three times to remove air thoroughly from the system. Finally, we filled the container with 1.8 bar CO_2 in the reactor. A 300-W Xe lamp (λ > 400 nm) was used as the light source with 450 mW/cm^2 optical density under room temperature. During 1 h irradiation with continuing stirring, 3 mL gas was sampled and analyzed by the Shimadzu GC 2014C

gas chromatography (GC) system with TCD and FID detectors with He as the carrier gas. The isotopic experiment using $^{13}CO_2$ under the same condition with gas chromatography-mass spectrometry (GC-MS, QP2020).

Photoelectrochemical measurements

All photoelectrochemical measurements were tested using CHI 760E electrochemical workstation with a standard three-electrode photoelectrochemical quartz cell (counter electrode, platinum (Pt) electrode; reference electrode, Ag/AgCl electrode) in 0.1 M Na_2SO_4 aqueous solution (electrolyte solution) at room temperature. The distance between the counter and working electrode was 2 cm. The indium Tin Oxide (ITO) loading with 1 cm × 1 cm area photocatalyst was served as a working electrode. Mott-Schottky test was also carried out in Na_2SO_4 solution (0.1 M). Photocurrent measurements of the synthesized photocatalysts were measured through several on-off cycles of light irradiation by a 300 W xenon lamp (using a 400 nm cutoff filter).

The photoelectrode preparations in this system were as follows: 25 mg of a powder sample was dispersed in a mixed solution with 0.3 mL of ethanol and 0.7 mL H_2O, the sample was ultrasonic for 48 h to make it evenly dispersed and then the obtained slurry was deposited as a thin film onto the ITO glass substrate within 1×1 cm area. When the slurry was almost dried thoroughly, 20 μL of Nafion solution (nafion:ethanol=1:3 v/v) was deposited on the ITO glass to obtain a homogeneous film.

Electrochemical tests

All electrochemical measurements were tested using CHI 760E electrochemical workstation with a standard three-electrode quartz electrochemical cell (counter electrode, platinum (Pt) electrode; reference electrode, Ag/AgCl electrode) in 1.0 M KOH aqueous solution (electrolyte solution) at room temperature. The distance between the counter and working electrode was 2 cm. The carbon-fiber paper loading 1.05 mg photocatalyst with 1 cm × 1 cm area was served as a working electrode. A series of cyclic voltammetry (CV) measurements to probe the electrochemical surface area (ECSA) were tested with different scan rates (10, 20, 30, 40, and 50 mV s^{-1}) from -0.10 to -0.15 V, and the sweep segments of the measurements were 50. All potentials were quoted to the reversible hydrogen electrode (NHE) and converted to NHE.

Computational details

The density of states (DOS) of the pristine 2H-MoS_2 slab, the oxygen-incorporated MoS_2 slab, pristine U-CoAl-LDH were calculated in Materials Studio.[4] A 3 × 3 × 2 supercell in the *a*-, *b*-, and *c*- directions was adopted for MoS_2 and CoAl-LDH, based on an initial structure with lattice parameters $\alpha = \beta = 90°$, $\gamma = 120°$. The lattice parameters *a*, *b*, and *c* were referred to the powder X-ray diffraction pattern obtained from experimental data. The molar ratio of Co^{2+}:Al^{3+} in the LDH matrix was 2. Carbonate anion was placed in the interlayer space of CoAl-LDH to keep the model neutral. The model of ultrathin CoAl-LDH was obtained by cleaving the (003) surface of CoAl-LDH. This model contained two bilayers of CoAl-LDH matrix and interlayer carbonate anion with vacuum widths of 15 Å. The values of U-J (U_{eff}) was 3.52 eV for Co ions and 0 eV for other ions.[5] The self-consistent field (SCF) tolerance was 1×10^{-5} eV and the Brillouin zone was sampled by 1 × 1 × 1 k-points. The core electrons were replaced with ultrasoft pseudopotentials.

Table S1. Comparison of photocatalytic CO_2 reduction performance for various photocatalysts in this work and in previous literature

Photocatalyst	Photosensitizer /Co-catalyst	Sacrificial agent	Solvent	Light source	Main product yield ($\mu mol \cdot h^{-1} \cdot g^{-1}$)	Reference
U-CoAl-LDH	$Ru(bpy)_3Cl_2 \cdot 6H_2O$	TEOA	MeCN-H_2O (3:1 v/v)	300 W Xe (λ > 400 nm)	CO: 8070 (49%) H_2: 8415 (51%)	This work
LDH/MoS_2 (0.2 - 1.5 mg/mL)	$Ru(bpy)_3Cl_2 \cdot 6H_2O$	TEOA	MeCN-H_2O (3:1 v/v)	300 W Xe (λ>400 nm)	H_2:CO = 1.3:1-15:1	This work
Co-ZIF-9	$Ru(bpy)_3Cl_2 \cdot 6H_2O$	TEOA	MeCN-H_2O (4:1 v/v)	300 W Xe (λ>420 nm)	CO: 41.8 (58.3%) H_2: 30.3 (41.7%)	Angew, 2014, 53, 1034[6]
Co_3O_4-400	$Ru(bpy)_3Cl_2 \cdot 6H_2O$	TEOA	MeCN-H_2O (3:1 v/v)	300 W Xe (λ>420 nm)	CO: 2003 (77.1%) H_2: 595 (22.9%)	Adv. Mater. 2016, 28, 6485[7]
C doped BN	$CoCl_2$ 2'2-bipyridine	TEOA	MeCN-H_2O (2:1 v/v)	300 W Xe (λ>420 nm)	CO: 9.3 (76.2%) H_2: 2.9 (23.8%)	Nat. Commun. 2015, 6, 7698[8]
Dye/TiO_2/Re(Ⅰ): Co(Ⅲ) complex (9:1)	Dye	BIH	DMF-H_2O (4:1 v/v)	60 W LED (λ>400)	CO: (76.9%) H_2: (23.1%)	Angew, 2017, 56, 976[9]
g-C_3N_4	$Co(bpy)_3^{2+}$	TEOA	MeCN-H_2O (4:1 v/v)	300 W Xe (λ>420 nm)	CO: 469 (81.83%) H_2: 104 (18.17%)	Appl. Catal. B, 2015, 179, 1[10]
Pt/C-In_2O_3	Pt	TEOA	H_2O-TEOA (9:1 v/v)	300 W Xe	CH_4: 139.5 (14.0%) CO: 633 (63.3%) H_2: 227.5 (22.7%)	JACS, 2017, 139, 4123[11]
In_2S_3-$CdIn_2S_4$	$Co(bpy)_3^{2+}$	TEOA	MeCN-H_2O (3:2 v/v)	300 W Xe (λ>400 nm)	CO: 825 (70.2%) H_2: 350 (29.8%)	JACS, 2017, 139, 17305[12]

$ZnIn_2S_4$–In_2O_3	$CoCl_2$ 2'2-bipyridine	TEOA	MeCN-H_2O (3:2 v/v)	300 W Xe (λ>400 nm)	CO: 3075 (75%) H_2: 800 (25%)	JACS, 2018, 140, 5037[13]
$CoSn(OH)_6$	$Ru(bpy)_3Cl_2 \cdot 6H_2O$	TEOA	MeCN-TEOA-H_2O 3:1:2 v/v	300 W Xe (λ>420 nm)	CO: (86.18%) H_2: (13.82%)	Appl. Catal. B, 2018, 224, 1009[14]
Co/C	$Ru(bpy)_3Cl_2 \cdot 6H_2O$	TEOA	MeCN-H_2O-TEOA (3:1:1 v/v/v)	300 W Xe (λ>450 nm)	CO: 448 (64.2%) H_2: 250 (35.8%)	Small, 2018, 14, 1800762[15]
MoO(dithiolene)$_2$ complex	$Ru(bpy)_3Cl_2 \cdot 6H_2O$	BIH	MeCN-TEOA (5:1 v/v)	300 W Xe (λ=400-1200 nm)	HCOOH: (39%) CO: (19%) H_2: (42%)	Angew, 2018, 57, 17033[16]
Zr-complex	$[Ru(phen)_3](PF_6)_2$	TEOA	MeCN	300 W Xe (λ=385-740 nm)	CO: (20.7%) HCOOH: (57.8%) H_2: (21.5%)	Angew, 2016, 55, 2697[17]
MAF-X27/-OH	$Ru(bpy)_3Cl_2 \cdot 6H_2O$	TEOA	MeCN-H2O (4:1 v/v)	LED (λ=420 nm)	CO: 45 (98.3%) H_2: 0.8 (1.7%)	JACS, 2018, 140, 38[18]

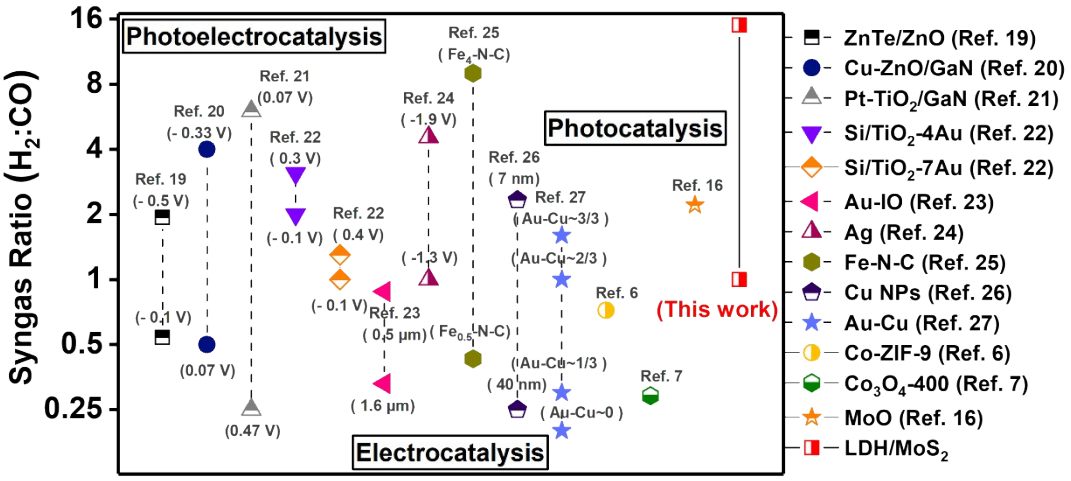

Fig. S1 The syngas ratio of H_2:CO on various catalysts in the references in the field of photoelectrocatalysis,[19-22] electrocatalysis[23-27] and photocatalysis[6, 7, 16], respectively, with dotted lines indicating the range of H_2:CO ratios.

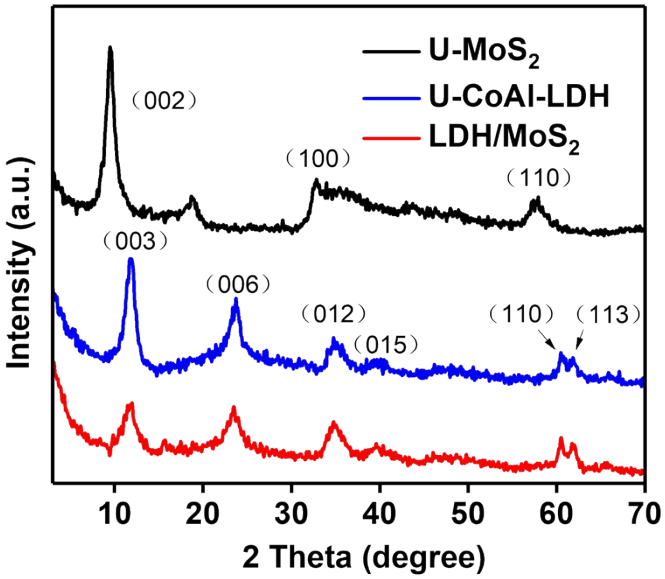

Fig. S2 XRD patterns of the synthesized U-MoS_2, U-CoAl-LDH and LDH/MoS_2 nanocomposite.

XRD technique was carried out on various samples to investigate the phase structure information and the results were shown in Fig. S2. For 1T-phase U-MoS_2, in the low angle, two peaks relative to d spacings of 9.50 Å and 4.75 Å, respectively, which were attributed to the (002) diffraction peak indicating that a layered structure for 1T-phase MoS_2. For U-CoAl-LDH, the reflections at 11.75°, 23.69°, 34.74°, 39.71°, 60.42°, and 61.81° were ascribed to the (003), (006), (012), (015), (110), and (113) lattice planes, respectively, indexed to the hexagonal CoAl-LDH (JCPDS No. 22-0452). The main peaks such as (003), (006) were still presented in LDH/MoS_2 after the combination of MoS_2 and CoAl-LDH which proved the successful synthesis of samples. Besides, the main peak of CoAl-LDH (003) in LDH/MoS_2 with decreased intensity, which due to the coordination between the two components in LDH/MoS_2 nanocomposite.

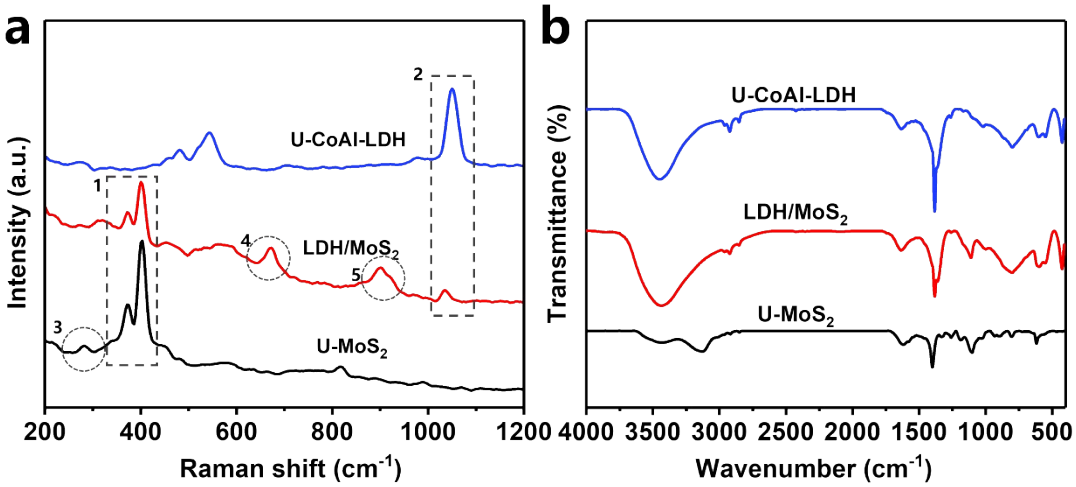

Fig. S3 (a) Raman and (b) Fourier transform infrared (FTIR) spectra of U-CoAl-LDH, LDH/MoS_2 and U-MoS_2.

As can be seen from the Raman spectra (Fig. S3a), the peaks located at 374 cm^{-1} and 402 cm^{-1} (number 1) can be attributed to the vibrational modes of Mo-S E^1_{2g} and A_{1g} in MoS_2 structure[28], while the peaks at 282 cm^{-1} (number 3) can be attributed to the B_{2g} vibrational modes of Mo-O bonds,[29] thus proving the oxygen incorporation in U-MoS_2. The peak located at 1049 cm^{-1} (number 2) can be attributed to CO_3^{2-} symmetric stretching vibration mode, which was the most characteristic peak of the interlayer structure in the CoAl-LDH. For LDH/MoS_2 nanocomposite, the peaks located at 672 cm^{-1} and 890 cm^{-1} were ascribed to Mo-O bending vibration and Mo-O-Mo stretching vibrations in the octahedron,[29] respectively, further indicating the coordination between the two components in LDH/MoS_2 nanocomposite. In the FTIR spectrum (Fig. S3b), the absorption at 1630, 3400-3500 cm^{-1} were identified as the bending and stretching vibration of H-O-H, respectively, in both U-MoS_2 and U-CoAl-LDH. The peak at 1355 cm^{-1} was attributed to the bending vibrations of CO_3^{2-} ions intercalated in the nanosheets[30] and below 900 cm^{-1} was attributed to the translational modes of M-O and M-OH.[31]

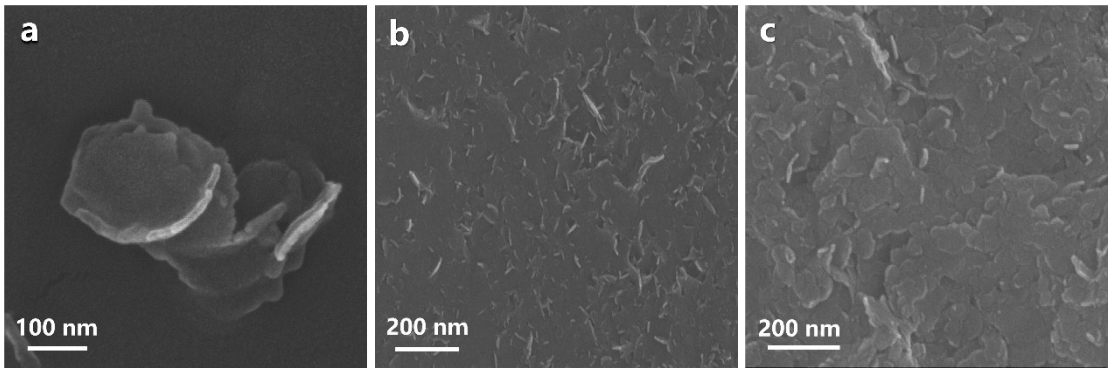

Fig. S4 SEM images of (a) U-MoS_2, (c) U-CoAl-LDH, (c) LDH/MoS_2.

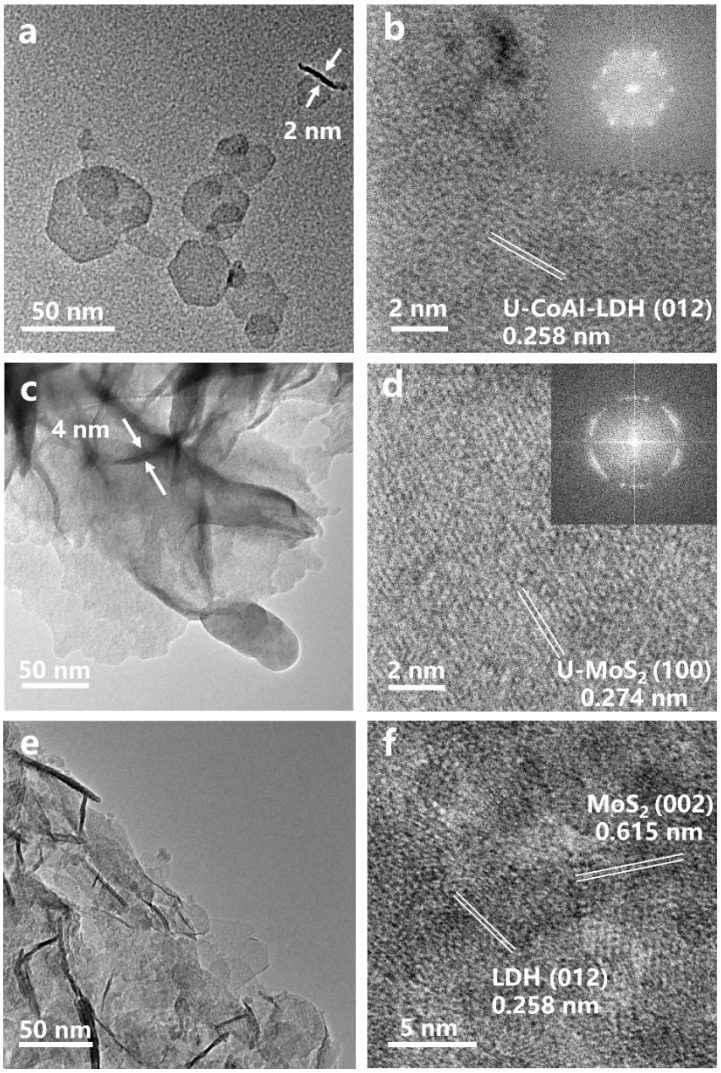

Fig. S5 TEM and HRTEM images of (a, b) U-CoAl-LDH, (c, d) U-MoS_2, (e, f) CoAl-LDH/MoS_2 nanocomposite.

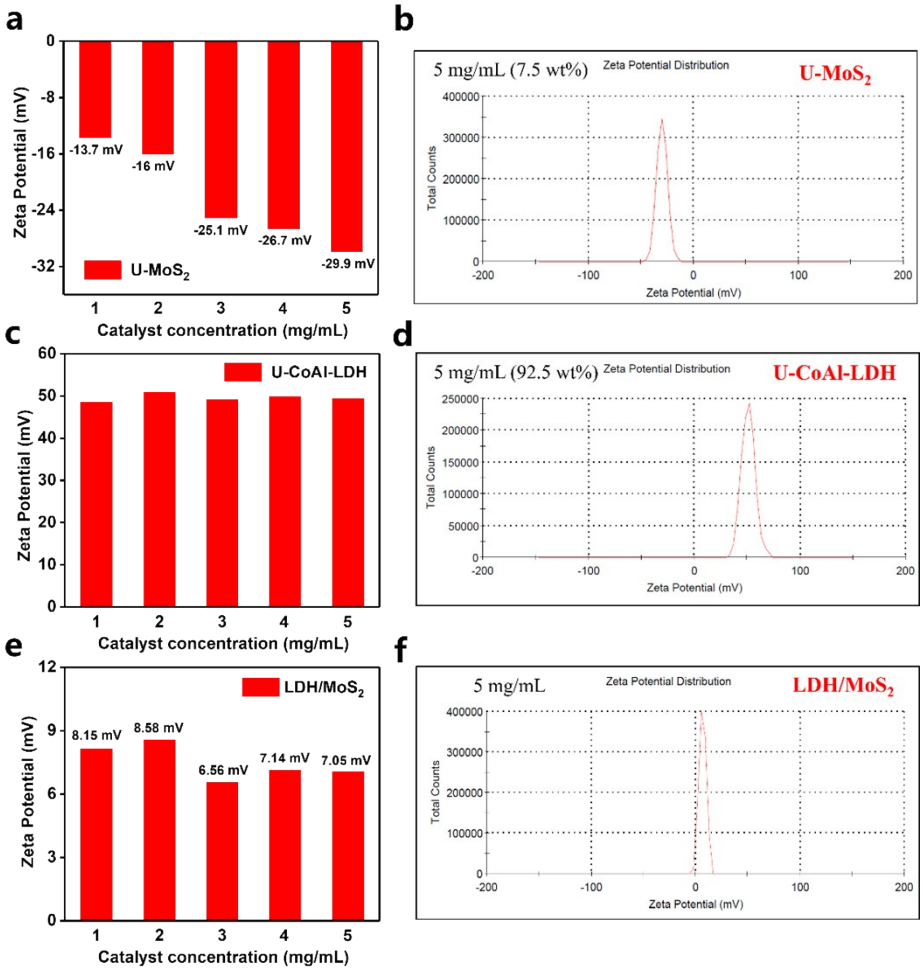

Fig. S6 Zeta potentials with (a) different concentration and (b) 5 mg/mL of U-CoAl-LDH (92.5 wt% of the total concentration); (c) different concentration and (d) 5 mg/mL U-MoS_2 (7.5 wt% of the total concentration); (e) different concentration and (f) 5 mg/mL LDH/MoS_2, samples dispersed in water.

The zeta potential was tested with water as solvent (Fig. S6). The zeta potentials of U-CoAl-LDH (92.5 wt%) were positive through concentration 1, 2, 3, 4, 5 mg/mL (+48.6 mV, +50.8 mV, 49.1 mV, 49.8 mV, +49.4 mV), the U-MoS_2 (7.5 wt%) were negative through different concentration 1, 2, 3, 4, 5 mg/mL (−13.7 mV, −16 mV, −25.1 mV, −26.7 mV, −29.9 mV) and the zeta potentials of LDH/MoS_2 nanocomposite after electrostatic interactions were positive through different concentration 1, 2, 3, 4, 5 mg/mL (+8.15 mV, +8.58 mV, 6.56 mV, 7.14 mV, +7.05 mV). It was found that the zeta potential of the LDH/MoS_2 nanocomposite had an obvious displacement relative to the CoAl-LDH and MoS_2 precursors from positive and negative, respectively, to near no charge, further revealing the successful combination between the two components in LDH/MoS_2 nanocomposite.

Table S2. Photocatalytic CO_2 reduction performance under same reaction system with different catalyst concentration

Catalyst concentration (mg/mL)	Catalyst	Yield (μmol/h)		Selectivity (%)		Syngas ratio H_2:CO
		CO	H_2	CO Sel.	H_2 Sel.	
0.2 × 92.5 wt%	U-CoAl-LDH	16.14	16.83	48.95	51.05	**1:1**
0.2	LDH/MoS_2	14.15	18.21	44.74	56.26	**1.3:1**
0.4	LDH/MoS_2	9.50	19.00	33.35	66.65	**2:1**
0.6	LDH/MoS_2	6.36	19.74	24.35	75.65	**3:1**
0.8	LDH/MoS_2	5.37	20.25	20.96	79.04	**4:1**
1.0	LDH/MoS_2	4.11	21.21	16.23	84.77	**5:1**
1.5	LDH/MoS_2	2.19	32.11	6.39	93.61	**15:1**
1.5 × 7.5 wt%	U-MoS_2	0.29	2.78	9.45	90.55	10:1

Reaction condition: photosensitizer: 4 × 10^{-6} mol $Ru(bpy)_3Cl_2·6H_2O$; Catalyst concentration: 0.2-1.5 mg/mL; solvent: 10 mL (CH_3CN/TEOA/H_2O = 3:1:1 (v/v)); λ > 400 nm, 1 h.

Table S3. Photocatalytic CO_2 reduction performance of different reaction system

Reaction system	Yield (μmol/h)		Selectivity (%)	
	CO	H_2	CO Sel.	H_2 Sel.
Normal condition ($Ru(bpy)_3Cl_2·6H_2O$ + Catalyst + TEOA + CO_2 + H_2O)	9.50	18.99	33.33	66.67
Without CO_2 ($Ru(bpy)_3Cl_2·6H_2O$ + Catalyst + TEOA + H_2O)	0	6.17	0	100
Without catalyst ($Ru(bpy)_3Cl_2·6H_2O$ + TEOA + CO_2 + H_2O)	0.28	1.24	18.42	81.58
Without TEOA ($Ru(bpy)_3Cl_2·6H_2O$ + Catalyst + CO_2 + H_2O)	0	0	0	0
In dark ($Ru(bpy)_3Cl_2·6H_2O$ + Catalyst + CO_2 + H_2O)	0	0	0	0
Without $Ru(bpy)_3Cl_2·6H_2O$ (LDH/MoS_2 + TEOA + CO_2 + H_2O)	0	0.15	0	100
Without $Ru(bpy)_3Cl_2·6H_2O$ (U-CoAl-LDH + TEOA + CO_2 + H_2O)	0	0	0	0
Without $Ru(bpy)_3Cl_2·6H_2O$ (U-MoS_2 + TEOA + CO_2 + H_2O)	0	0.05	0	100

Reaction condition: photosensitizer: 4×10^{-6} mol $Ru(bpy)_3Cl_2·6H_2O$; Catalyst: LDH/MoS_2; Catalyst concentration: 0.4 mg/mL; solvent: 10 mL (CH_3CN/TEOA/H_2O = 3:1:1 (v/v)); $\lambda > 400$ nm, 1 h.

It can be shown that there were almost no activity with CoAl-LDH or MoS_2 alone in the absence of photosensitizer Ru complex. Besides, the CO_2 conversion was also rather low with only $[Ru(bpy)_3]Cl_2·6H_2O$ used in the control experiment which exhibited the $Ru(bpy)_3Cl_2$ and heterostructured LDH-MoS_2 combined together can undergo selective photoreduction of CO_2 with H_2O to CO and H_2. $[Ru(bpy)_3]Cl_2·6H_2O$ is widely used as a photosensitizer in CO_2 photocatalytic reduction studies. It can be photoexcited under light irradiation, with the photoexcited electrons then being transferred to the surface of photocatalyst for the further CO_2 reduction.

Table S4. Photocatalytic CO_2 reduction performance under same reaction system with different catalyst concentration under $\lambda > 500$ nm

Catalyst concentration (mg/mL)	Catalyst	Yield (μmol/h)		Selectivity (%)		Syngas ratio H_2:CO
		CO	H_2	CO Sel.	H_2 Sel.	
0.2	LDH/MoS_2	9.15	15.35	37.34	62.66	**1.7:1**
0.4	LDH/MoS_2	7.99	15.93	33.41	66.59	**2:1**
0.6	LDH/MoS_2	6.26	16.79	27.15	72.85	**2.7:1**
0.8	LDH/MoS_2	4.76	17.58	21.30	78.70	**3.7:1**
1.0	LDH/MoS_2	3.75	18.27	17.02	82.98	**4.9:1**
1.5	LDH/MoS_2	1.40	25.27	5.27	94.73	**18:1**

Reaction condition: photosensitizer: 4×10^{-6} mol $Ru(bpy)_3Cl_2 \cdot 6H_2O$; Catalyst concentration: 0.2-1.5 mg/mL; solvent: 10 mL (CH_3CN/TEOA/H_2O = 3:1:1 (v/v)); $\lambda >$ 500 nm, 1 h.

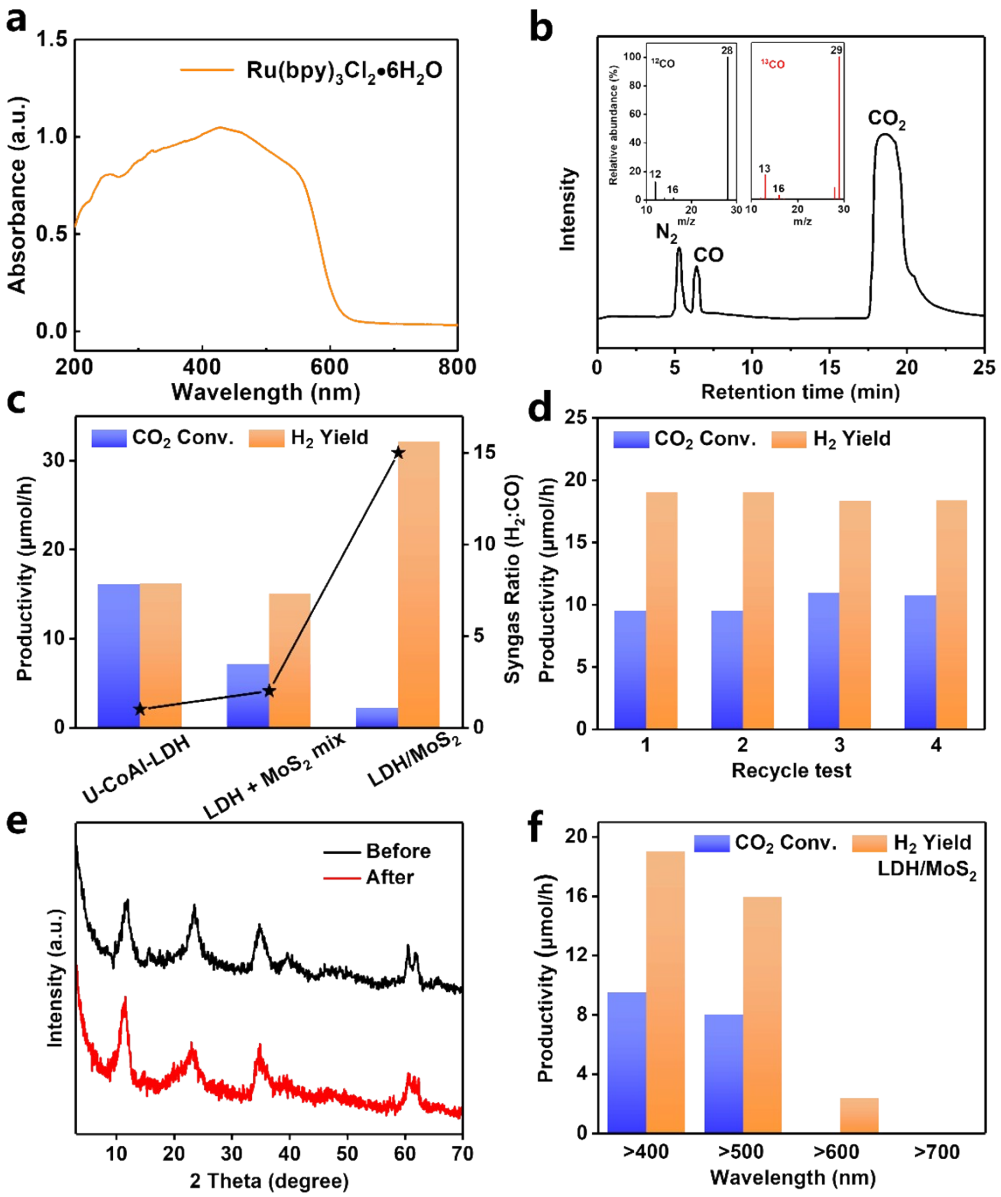

Fig. S7 (a) The UV-vis spectrum of the photosensitizer $Ru(bpy)_3Cl_2 \cdot 6H_2O$ adapted from our previous work;[32] (b) GC spectrum (connected to MS) of the reaction products using LDH/MoS_2 as the photocatalyst, the insert showed the mass spectra of CO generated using $^{12}CO_2$ or $^{13}CO_2$ as the reactant, respectively; The production rate and syngas ratio of H_2:CO in CO_2PR; (c) for 1.5 mg/mL LDH + MoS_2 mix and LDH/MoS_2; (d) using 0.4 mg/mL recycled LDH/MoS_2 (λ > 400 nm); (e) characterization of LDH/MoS_2 XRD pattern in contrast of the fresh and after the recycled sample; (f) using 0.4 mg/mL LDH/MoS_2 under irradiation with different wavelength; (Reaction condition: photosensitizer: 4×10^{-6} mol $Ru(bpy)_3Cl_2 \cdot 6H_2O$; solvent: 10 mL ($CH_3CN$/TEOA/$H_2O$ = 3/1/1 (v/v/v)); 1 h).

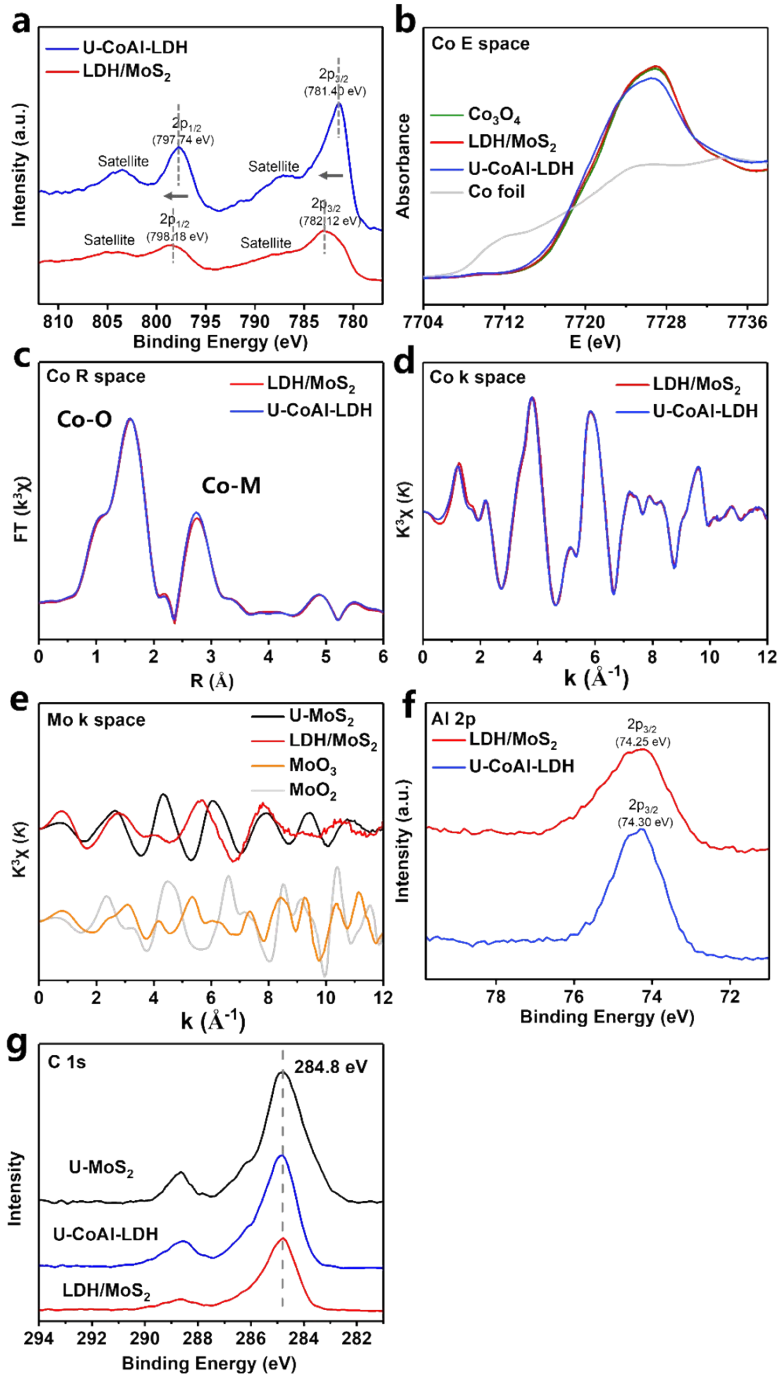

Fig. S8 (a) XPS profiles of Co 2p with U-CoAl-LDH and LDH/MoS_2 nanocomposite; (b) Co K-edge X-ray absorption near edge structure (XANES) spectra; (c) Co magnitude of weighted FT of K-edge extended X-ray absorption fine-structure(EXAFS); (d) Co K-edge EXAFS Oscillation function $k^3\chi(k)$ of U-CoAl-LDH, LDH/MoS_2; (e) Mo K-edge EXAFS Oscillation function $k^3\chi(k)$ of U-MoS_2, LDH/MoS_2, MoO_2, MoO_3, respectively; (f) XPS profiles of Al 2p of U-CoAl-LDH and LDH/MoS_2 nanocomposite, respectively; (g) C 1s spectra for U-MoS_2, U-CoAl-LDH and LDH/MoS_2 nanocomposite, respectively.

As shown in Fig. S8g, all the XPS spectra were calibrated against the C 1s peak of adventitious hydrocarbons at 284.8 eV.

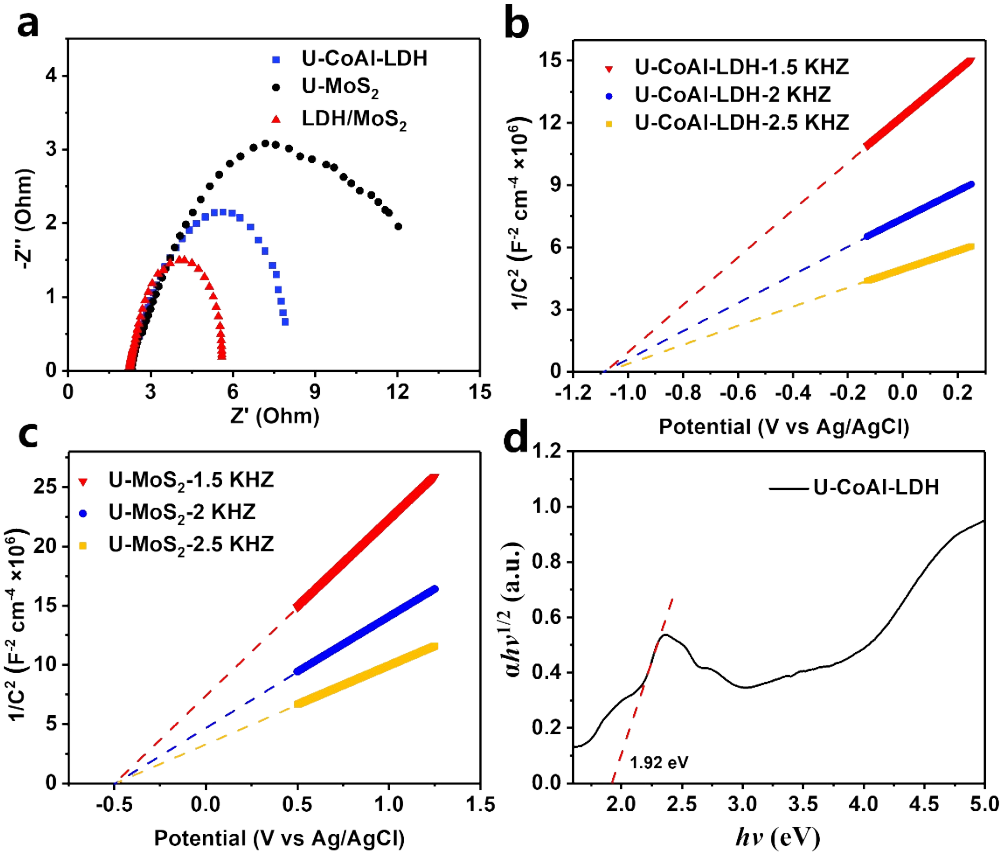

Fig. S9 (a) Electrochemical impedance spectra; (b, c) Mott-Schottky plots of U-CoAl-LDH, and U-MoS_2, respectively; (d) the band gap calculation of U-CoAl-LDH from the Kubelka-Munk function and Tauc plot $(\alpha hv)1/n = A(hv - E)$.

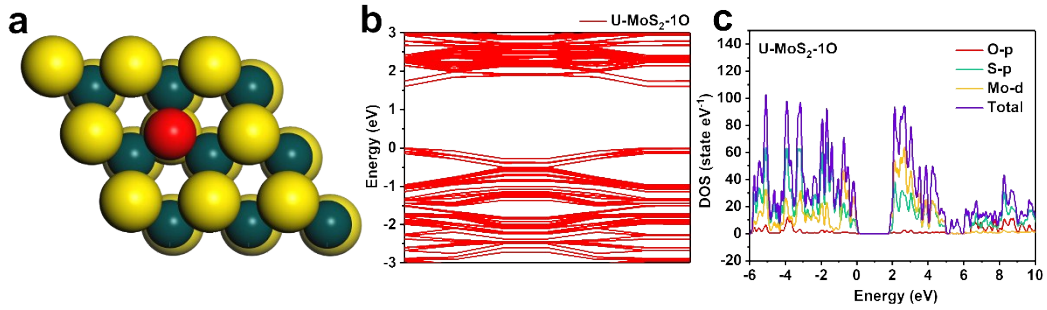

Fig. S10 (a) Schematic structure, (b) band gap and (c) the corresponding calculated DOS plots for MoS_2 with O incorporated of the as built model (dark green, yellow and red corresponding to Mo, S and O atoms, respectively).

As shown in the calculated density of states (DOS) in Fig. S10, a 3 × 3 × 2 supercell of MoS_2 with O incorporated in model as reported[2] were built and the band gap of them was calculated by DOS (the density of states) in Materials Studio with the results of 1.604 eV.

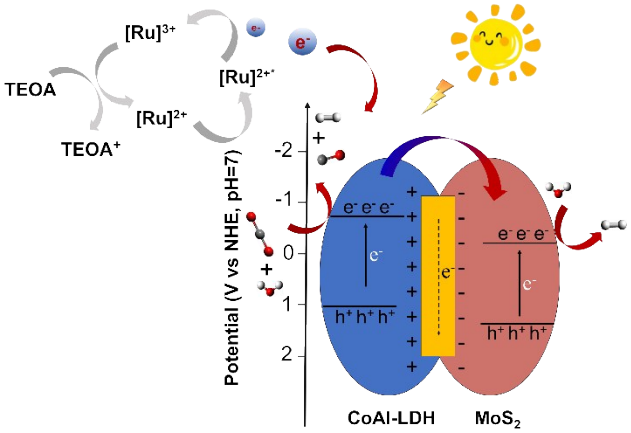

Fig. S11 Schematic illustration of the proposed mechanism for photocatalytic CO_2 reduction under visible light irradiation (Ru^{3+} represents as Ru-complex; O, C and H atoms are represented by red, grey and white spheres, respectively). [33, 34]

Reference

1. J. Yu, B. R. Martin, A. Clearfield, Z. Luo and L. Sun, *Nanoscale*, 2015, **7**, 9448-9451.
2. J. Xie, J. Zhang, S. Li, F. Grote, X. Zhang, H. Zhang, R. Wang, Y. Lei, B. Pan and Y. Xie, *J. Am. Chem. Soc.*, 2013, **135**, 17881-17888.
3. B. Ravel and M. Newville, *J. Synchrotron Radiat.*, 2005, **12**, 537-541.
4. S.-M. Xu, H. Yan and M. Wei, *J. Phys. Chem. C*, 2017, **121**, 2683-2695.
5. P. Liao, J. A. Keith and E. A. Carter, *J. Am. Chem. Soc.*, 2012, **134**, 13296-13309.
6. S. Wang, W. Yao, J. Lin, Z. Ding and X. Wang, *Angew. Chem. Int. Ed.*, 2014, **53**, 1034-1038.
7. C. Gao, Q. Meng, K. Zhao, H. Yin, D. Wang, J. Guo, S. Zhao, L. Chang, M. He, Q. Li, H. Zhao, X. Huang, Y. Gao and Z. Tang, *Adv. Mater.*, 2016, **28**, 6485-6490.
8. C. Huang, C. Chen, M. Zhang, L. Lin, X. Ye, S. Lin, M. Antonietti and X. Wang, *Nat. Commun.*, 2015, **6**, 7698.
9. J. S. Lee, D. I. Won, W. J. Jung, H. J. Son, C. Pac and S. O. Kang, *Angew. Chem. Int. Ed.*, 2017, **56**, 976-980.
10. J. Qin, S. Wang, H. Ren, Y. Hou and X. Wang, *Appl. Catal. B: Environ.*, 2015, **179**, 1-8.
11. Y. X. Pan, Y. You, S. Xin, Y. Li, G. Fu, Z. Cui, Y. L. Men, F. F. Cao, S. H. Yu and J. B. Goodenough, *J. Am. Chem. Soc.*, 2017, **139**, 4123-4129.
12. S. Wang, B. Y. Guan, Y. Lu and X. W. D. Lou, *J. Am. Chem. Soc.*, 2017, **139**, 17305-17308.
13. S. Wang, B. Y. Guan and X. W. D. Lou, *J. Am. Chem. Soc.*, 2018, **140**, 5037-5040.
14. X. Lin, Y. Gao, M. Jiang, Y. Zhang, Y. Hou, W. Dai, S. Wang and Z. Ding, *Appl. Catal.*

B: Environ., 2018, **224**, 1009-1016.

15. K. Zhao, S. Zhao, C. Gao, J. Qi, H. Yin, D. Wei, M. F. Mideksa, X. Wang, Y. Gao, Z. Tang and R. Yu, *Small*, 2018, **14**, 1800762.
16. T. Fogeron, P. Retailleau, L. M. Chamoreau, Y. Li and M. Fontecave, *Angew. Chem. Int. Ed.*, 2018, **57**, 17033-17037.
17. T. Kajiwara, M. Fujii, M. Tsujimoto, K. Kobayashi, M. Higuchi, K. Tanaka and S. Kitagawa, *Angew. Chem. Int. Ed.*, 2016, **55**, 2697-2700.
18. Y. Wang, N. Y. Huang, J. Q. Shen, P. Q. Liao, X. M. Chen and J. P. Zhang, *J. Am. Chem. Soc.*, 2018, **140**, 38-41.
19. Y. J. Jang, J.-W. Jang, J. Lee, J. H. Kim, H. Kumagai, J. Lee, T. Minegishi, J. Kubota, K. Domen and J. S. Lee, *Energ. & Environ. Sci.*, 2015, **8**, 3597-3604.
20. S. Chu, S. Fan, Y. Wang, D. Rossouw, Y. Wang, G. A. Botton and Z. Mi, *Angew. Chem. Int. Ed.*, 2016, **55**, 14262-14266.
21. S. Chu, P. Ou, P. Ghamari, S. Vanka, B. Zhou, I. Shih, J. Song and Z. Mi, *J. Am. Chem. Soc.*, 2018, **140**, 7869-7877.
22. C. Li, T. Wang, B. Liu, M. Chen, A. Li, G. Zhang, M. Du, H. Wang, S. F. Liu and J. Gong, *Energ. & Environ. Sci.*, 2019, **12**, 923-928.
23. A. S. Hall, Y. Yoon, A. Wuttig and Y. Surendranath, *J. Am. Chem. Soc.*, 2015, **137**, 14834-14837.
24. Y. C. Li, D. Zhou, Z. Yan, R. H. Gonçalves, D. A. Salvatore, C. P. Berlinguette and T. E. Mallouk, *ACS Energy Lett.*, 2016, **1**, 1149-1153.
25. T. N. Huan, N. Ranjbar, G. Rousse, M. Sougrati, A. Zitolo, V. Mougel, F. Jaouen and M. Fontecave, *ACS Catal.*, 2017, **7**, 1520-1525.
26. B. Kumar, J. P. Brian, V. Atla, S. Kumari, K. A. Bertram, R. T. White and J. M. Spurgeon, *Catal. Today*, 2016, **270**, 19-30.
27. M. B. Ross, C. T. Dinh, Y. Li, D. Kim, P. De Luna, E. H. Sargent and P. Yang, *J. Am. Chem. Soc.*, 2017, **139**, 9359-9363.
28. C. Lee, H. Yan, L. Brus, T. Heinz, J. Hone and S. Ryu, *Adv. Funct. Mater.*, 2012, **22**, 1385.
29. L. Seguin, M. Figlarz, R. Cavagnat and J.-C. Lassègues, *Spectrochim. Acta. A*, 1995, **51**, 1323-1344.
30. J. T. Kloprogge, D. Wharton, L. Hickey and R. L. Frost, *Am. Mineral.*, 2002, **87**, 623-629.
31. L. H. Chagas, G. S. G. De Carvalho, W. R. Do Carmo, R. A. S. San Gil, S. S. X. Chiaro, A. A. Leitão, R. Diniz, L. A. De Sena and C. A. Achete, *Mater. Res. Bull.*, 2015, **64**, 207-215.
32. L. Tan, S. M. Xu, Z. Wang, Y. Xu, X. Wang, X. Hao, S. Bai, C. Ning, Y. Wang, W.

Zhang, Y. K. Jo, S. J. Hwang, X. Cao, X. Zheng, H. Yan, Y. Zhao, H. Duan and Y. F. Song, *Angew. Chem. Int. Ed.*, 2019, **58**, 11860-11867.

33. P. Lang, R. Giereth, S. Tschierlei and M. Schwalbe, *Chem. Commun.*, 2019, **55**, 600-603.

34. Q. Li, F. Lin, F. Liu and X. Wang, *Chem. Commun.*, 2019, **55**, 3903-3906.